Quantitative aspects of infrared external reflection spectroscopy: Polymer/glassy carbon interface

ARTICLE *in* ANALYTICAL CHEMISTRY · OCTOBER 1986

Impact Factor: 5.64 · DOI: 10.1021/ac00125a023

4 AUTHORS, INCLUDING:

Marc Porter
University of Utah
198 PUBLICATIONS **14,127** CITATIONS
SEE PROFILE

David L Allara
Pennsylvania State University
261 PUBLICATIONS **23,138** CITATIONS
SEE PROFILE

Quantitative Aspects of Infrared External Reflection Spectroscopy: Polymer/Glassy Carbon Interface

Marc D. Porter,*[1] Thomas B. Bright, and David L. Allara*

Bell Communications Research, 600 Mountain Avenue, Murray Hill, New Jersey 07974

Theodore Kuwana*

Center for Bioanalytical Research and Department of Chemistry, University of Kansas, Lawrence, Kansas 66046

The quantitative aspects of infrared external reflection spectroscopy (IR-ERS) for the characterization of thin polymer films (<0.5 μm) on glassy carbon (GC) have been developed. Classical electromagnetic theory has been applied to calculate the mean-square electric field (MSEF) as a function of angle of incidence, polarization, and substrate optical properties. These data were used to determine conditions for optimum sensitivity. Maximum MSEF occur at 60° from the surface normal for p-polarized light and at normal incidence for s-polarized light. Spectral band shapes due to the low reflectivity of GC for films of poly(methyl methacrylate) (PMMA) at GC are severely distorted with respect to those for transmission spectra. For example, the band shape for the carbonyl stretch for a 78-Å PMMA film, analyzed with p-polarized irradiation that was incident at 60°, is very asymmetric with an absorption maximum shifted several wavenumbers higher in energy. Irradiation at 20° with s-polarized light results in derivative-like band shapes that strongly resemble the mirror-image of the anomalous dispersion of the real part of the PMMA refractive index. Integrated absorption strengths for spectra calculated via the parallel layer model for classical electromagnetic theory agree, in almost every instance, to within about 7% of those measured; absorbance maxima and minima agree to within 1-2 cm^{-1}. This agreement indicates that the observed distortions result from the inherent differences between ERS and transmission measurements and, more importantly, demonstrates the quantitative capabilities of IR-ERS.

In recent years carbon-based electrodes, such as glassy carbon (GC) and pyrolytic graphite, have received considerable attention based on their potential as replacements for precious metal electrodes (*1*, *2*). In most instances, however, these electrodes require some form of chemical and/or physical surface pretreatment in order to attain the desired electrochemical properties. Examples of such pretreatments include mechanical abrasion, covalent attachment, adsorption of an electrochemically active molecule directly to the electrode surface or overcoating with a thin film of a redox, ion-exchange, or semipermeable polymer (*3-9*). Essential to understanding the fundamental role of these surfaces in the electrochemical process is the ability to characterize the surface at both a qualitative (molecular) and quantitative level. Several vibrational spectroscopic techniques that probe the molecular nature of surfaces are currently available (*1*). Few studies, however, have applied the capabilities of infrared external reflection spectroscopy (IR-ERS) for such characterizations at carbon-based surfaces (*10*, *11*). This is a consequence of the inherent complexities of the experiment and the resulting spectra due to the lower reflectivity of carbon-based electrodes relative to metals. The low reflectivity reduces the sensitivity (*10*, *11*) and should also magnify the small band shape distortions that are observed for grazing incidence measurements at metals (*12*, *13*).

In this article we show that the complexities for the application of IR-ERS to GC can be reduced by combining the advantages of Fourier transform IR spectroscopy with considerations (*12*, *14-21*) based on classical electromagnetic theory. To demonstrate the capabilities and to assess the quantitative aspects for the application of IR-ERS to low surface area materials, we have examined thin (<0.5 μm) poly(methyl methacrylate) (PMMA) films at GC (PMMA/GC). PMMA was selected based on the ease with which its thickness could be controlled via spin-coating techniques and the isotropic nature of the resulting interfacial structure (*22*). In addition, comparisons with a previous study (*13*) of PMMA films at gold allow an assessment of the effects of the differences in substrate optical properties on the spectra. The experimental conditions for optimum sensitivity were calculated via classical electromagnetic theory. These results show that spectra can be obtained at a reasonable signal-to-noise ratio (although markedly distorted relative to band shapes for IR-ERS at metals and analogous transmission measurements) for film thicknesses near those of long alkyl chain monolayers. More importantly, the quantitative capabilities of IR-ERS are demonstrated by comparisons of observed spectra of the carbonyl stretching band of PMMA with those calculated via classical electromagnetic theory and the experimentally determined optical functions. These comparisons show differences that, in most instances, are less than 7% for several PMMA thicknesses and experimental conditions (angle of incidence and polarization). The applicability of quantitative IR-ERS to other low surface area interfaces is also discussed.

EXPERIMENTAL SECTION

Preparation of the PMMA/GC Films. The PMMA films (Polysciences, Inc., Warrington, PA) were cast onto GC-20 (Tokai Carbon Co., Tokyo, Japan) by spin-coating techniques. Sheets of GC were cut to provide plates that were approximately 2.5 by 2.5 cm. The plates were polished successively with slurries of 600-grit silicon powder and 3 μm, 1 μm, and 0.05 μm alumina (Buehler, Ltd., Evanston, IL) until a mirrorlike finish was obtained. Between each polishing step, the GC was washed in an ultrasonic bath with doubly distilled water.

The films were prepared by flooding the surface with polymer solution and spinning at 1000-2000 rpm. Typical PMMA concentrations were 0.1-5.0% w/v in chlorobenzene (Burdick and Jackson Laboratories, Inc., Muskegon, MI). Residual solvent was removed by annealing in vacuo at 110 °C.

Film thicknesses were determined with a Rudolph 423 null-point ellipsometer (Rudolph and Sons, Inc., Fairfield, NJ) at 6328

[1] Present address: Department of Chemistry, Iowa State University, Ames, IA 50011.

0003-2700/86/0358-2461$01.50/0

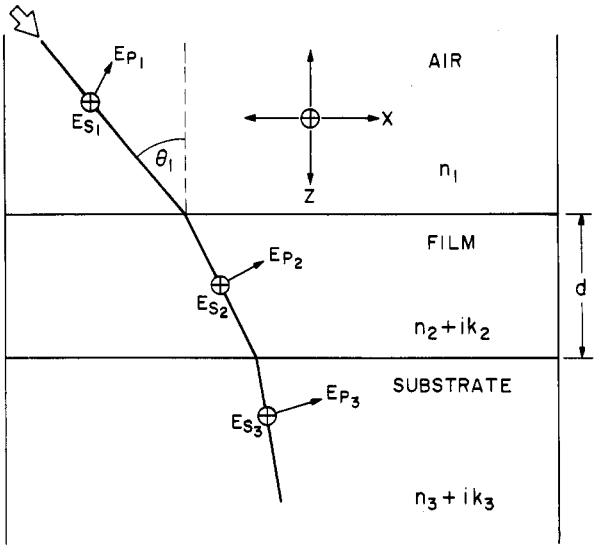

Figure 1. Electric field components and angle of incidence for a three-phase isotropic medium (see text). The reflected components are omitted for simplicity.

Å and/or a Sloan Dectak IIA surface profiler (Sloan Instruments, Santa Barbara, CA). For the surface profiler measurements, a knife edge was used to remove several portions of the film from the substrate with the resulting step used for the thickness measurements. Thicknesses were measured at three different locations on each film; the resulting thicknesses are given as the average and the uncertainty reported as the range of these measurements.

Instrumentation. Spectra were obtained with either a Digilab Model 15B or 15E Fourier transform IR spectrometer (Biorad, Cambridge, MA). For the reflection measurements the optics were modified to provide an ~f/15 beam (*23*). An aluminum wire grid polarizer on KRS-5 (Cambridge Physical Sciences), placed immediately before the sample, provided polarization selection. Spectra were obtained in a single reflection mode with a liquid N_2 cooled, broad-band HgCdTe detector (Infrared Associates, NJ). The moving mirror speed was 1.4 cm/s. After triangular apodization, the spectral resolution was 2 cm^{-1}. All sample spectra were referenced to their respective bare substrates. The spectrometer was purged with N_2 gas, which was passed through molecular sieve and charcoal traps to minimize water vapor and CO_2. The reflection spectra are the ratio of 800 sample to 800 reference scans.

Three-Phase Isotropic and Parallel Layer Model for the Glassy Carbon Interface. The structure of the PMMA/GC was modeled as an optically isotropic three-phase medium that consisted of parallel boundaries. This model and the electric field components due to the incident light are shown in Figure 1. The entry phase is transparent, whereas the refractive indexes for the second and third phases are complex, $\hat{n}_j = n_j + ik_j$ (n_j is the real index of refraction and k_j is the extinction coefficient for phase j). Phase 2, the PMMA film, is further defined by its thickness, d. The electric field components, E_z and E_x, are in the plane of incidence (p-polarized); E_y is perpendicular to the plane of incidence (s-polarized). It should be noted that E_z is perpendicular to the PMMA/GC interface, whereas E_x and E_y are parallel to this interface. The angle of incidence, θ_1, is given with respect to the surface normal.

Method of Calculating Mean-Square Electric Fields and Reflection Spectra. Several two-, three-, and n-phase formulations, based on boundary value solutions of Maxwell's equations, have been derived for calculating MSEF and reflection spectra (*14–19*). Inputs for these calculations include θ_1, $\hat{n}_j$ for each phase, the thicknesses for the intermediate phase(s), and the polarization of the incident light. Algorithms for these calculations have been previously described (*9*, *13*, *24*).

Complex Refractive Index of PMMA. The $\hat{n}_2$ for the carbonyl stretching region of PMMA is shown in Figure 2. These values were determined by a computational method that estimates an initial value for k_2 from a transmission spectrum for a thin

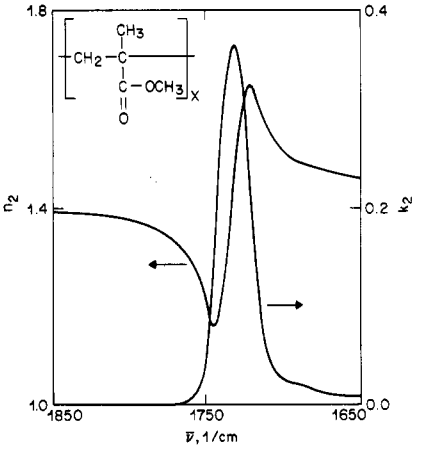

Figure 2. Complex refractive index for PMMA in the carbonyl stretching region.

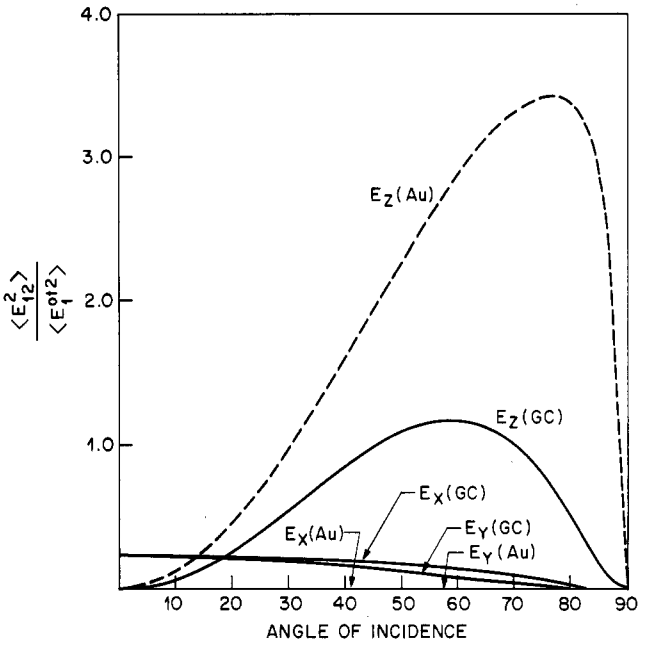

Figure 3. The mean-square electric field at 2000 cm^{-1} as a function of angle of incidence and polarization at the air/GC (——) and air/Au interface (– – –) for GC, $\hat{n}$ = 2.9 + 1.3i (*27*), and for Au, $\hat{n}$ = 2.7 + 28.5i (*28*).

PMMA film and, then, by Kramers–Kronig analysis iteratively approaches a solution for n_2 and k_2 at a preset convergence limit. This algorithm has been previously described (*24*). A value of 1.42 was used for n_∞ (*13*). As shown in Figure 2, k_2 has a maximum at 1731 cm^{-1} and a full width at half maximum that is slightly less than 15 cm^{-1}. The band on the low energy side of the k_2 maximum results from C=O that is hydrogen bonded with H_2O. The n_2 varies in the usual anomalous or derivative-like fashion in this region and has a minimum of almost 1.2 at 1720 cm^{-1} and a maximum of approximately 1.6 at 1746 cm^{-1}. These data agree with those previously published (*13*, *25*).

RESULTS AND DISCUSSION

Comparison of Conditions for Optimum Sensitivity at Metal and Semiconductor Interfaces. The dependence of the surface sensitivity of IR-ERS on the angle of incidence and polarization of the incoming light at metal interfaces is well-known (*14–21*). Basically, the sensitivity is governed by the boundary conditions imposed by the free electrons of the metal substrate. This results in near-zero values for E_x and E_y at the interface for all angles of incidence. The component perpendicular to the interface, however, has large values at large angles of incidence. Figure 3 is a plot of the relative intensity of the MSEF at air/Au (given as the ratio of the

MSEF at the interface, $\langle E_{12}^2 \rangle$, to the MSEF of the incident field, $\langle E_1^{ot2} \rangle$) and air/GC vs. angle of incidence and polarization at 2000 cm^{-1}. The optical constants for Au and GC were extrapolated from previous studies (*26*, *27*). Figure 3 shows that the MSEF for E_x and E_y at air/Au are negligibly small (<0.004) for all angles of incidence. In contrast, the MSEF for E_z is zero at normal incidence, increases with θ_1 to a maximum of approximately 3.4 at 79°, and then rapidly returns to zero. Hence, from the standpoint of available excitation energy, conditions for high sensitivity are large angles of incidence with p-polarized light. It should be noted that the anisotropic nature of the MSEF results in the selective excitation of vibrations with dipole derivatives that have components perpendicular to the interface. This preferential excitation (*15*), commonly known as the IR surface selection rule, has been exploited to develop orientational descriptions for organized monolayer structures at metals (*24*, *28–30*).

In contrast to metallic reflection, the lower conductivity of GC (approximately 200 Ω^{-1} cm^{-1} at 25 °C (*31*)) results in a less efficient screening of the incident electric field. Hence, as shown in Figure 3, the MSEF at air/GC are markedly different from those at air/Au. At air/GC, the MSEF for E_x and E_y are roughly 0.25 at normal incidence and slowly decrease as θ_1 increases. The MSEF for E_z reaches a maximum of almost 1.2 (less than 1/3 the maximum value at air/Au) at 60°; the MSEF for E_x at this angle equals 0.15. If only differences in MSEF are considered, the optimum sensitivity at air/GC should then be about 0.13 times that at air/Au. Detailed considerations, as discussed below, for a thin film (finite collection of oscillators) depend, of course, on additional factors such as the refractive index of phase 2 (screening induced by the film) and the irradiated surface area. It should also be noted that at 60° p-polarized light excites vibrations with dipole derivatives that have components perpendicular and/or parallel to the air/GC interface. This mixing of excitation complicates a spectral interpretation in terms of an oriented surface structure.

Band Shape and Intensity Distortions for IR-ERS Measurements at GC. In addition to the sensitivity and interpretation considerations that result from the anisotropic nature of the MSEF at air/GC, several other underlying factors that affect band shapes require examination before, for example, assigning differences between IR-ER and transmission spectra to surface-induced changes in structure and/or chemical bonding. These factors include effects of the reflectivity at phase 1/phase 2 (R_{12}) and the periodicity of the MSEF in phase 2. For small values of k_2, R_{12} changes due to the anomalous dispersion of n_2. With increasing n_2, the contribution of R_{12} to the spectrum will be greater on the low energy side of the k_2 maximum. This results in a band that has an absorbance maximum shifted toward higher energies and an asymmetric shape. It should be noted that the variation of R_{12} also alters the net MSEF in phase 2.

The shape and intensity of the IR-ER spectra are also distorted by the periodicity of the MSEF in phase 2. The periodicity, which is essentially that of a dampened standing wave, is given by $x = (2\bar{\nu}n_2 \cos \theta_1)^{-1}$, where x represents the distance between adjacent nodes or antinodes. This equation shows that x is inversely proportional to both $\bar{\nu}$ and n_2. This means that as $\bar{\nu}$ increases the standing wave contracts (x decreases), concentrating the MSEF in phase 2. In contrast, a decrease in $\bar{\nu}$ expands the standing wave (x increases); this reduces the MSEF in phase 2. Overall, these considerations indicate that the band shapes and intensities result from a mixture of contributions from both k_2 and n_2.

The effects of the above factors on IR-ER band shapes and intensities for thin PMMA films at Au have been investigated (*13*). This study also examined the effects of the angle of incidence and polarization for several PMMA thicknesses. Comparisons between observed spectra for the carbonyl stretching mode and those expected for transmission measurements indicated that, in general, the band shapes for the IR-ER spectra are very asymmetric and the absorbance maxima are shifted 10–15 cm^{-1} higher in energy than in the transmission measurements. IR-ER spectra calculated via classical electromagnetic theory demonstrated that the asymmetry resulted primarily from the effects of the dispersion of n_2.

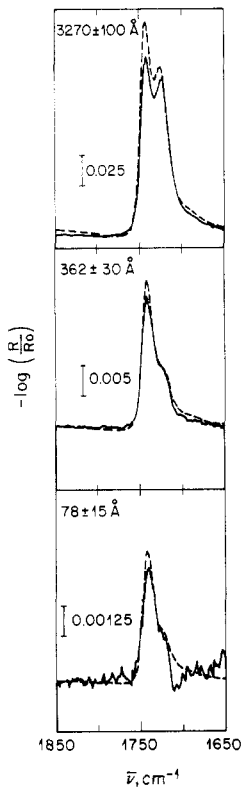

Figure 4. Experimental (——) and calculated (– – –) IR-ER spectra for PMMA films of various thicknesses at GC: 3270 ± 100 Å; 362 ± 30 Å; and 78 ± 15 Å. The p-polarized light is incident at 60°.

In addition to the factors at metals, the low reflectivity of GC gives rise to other considerations that could produce IR-ER band distortions. Such distortions can be understood by examining the differences in the MSEF at air/GC relative to air/Au. As shown in Figure 3, the MSEF for E_x at GC is more than 35 times larger than that at Au for $\theta_1 = 60°$. This means that the contribution of n_2 to spectra at GC will be much larger than that at Au. Hence, band shapes for films at GC are further distorted due to the "mixing" of the MSEF periodicity in phase 2 and R_{12}. Similar considerations indicate that band shapes for s-polarized light are strongly controlled by the disperison of n_2.

IR-ER Spectra for PMMA/GC. Band Shape Distortions. The effects of experimental conditions on surface sensitivity and band shape and intensity distortions were assessed by using PMMA films of various thicknesses at GC. As stated earlier, PMMA was selected based on the ability to control its film thicknesses and its isotropic structure as a thin film. Hence, the comparison of the observed and calculated spectra provided the criterium for assessing the quantitative aspects of IR-ERS. Several experimental conditions were examined, based on the MSEF data in Figure 3. Figure 4 shows the observed and calculated spectra in the carbonyl stretching region for three PMMA films at GC with average thicknesses of 3270 ± 100, 380 ± 30, and 78 ± 15 Å. The p-polarized light was incident at 60°. The ordinate is given as the $-\log (R/R_0)$ where R is the reflectivity for

Table I. Observed and Theoretical[a] IR-ERS Data for Thin Films of PMMA at GC: Comparison of Peak Position and Integrated Absorption Strengths for the Carbonyl Stretching Band at Various Angles of Incidence and Polarizations

film thickness,[b] Å	angle of incidence, deg	polarization	peak positions,[c] cm^{-1} maximum[d] obsd	maximum[d] theory	minimum obsd	minimum theory	integrated absorption[f] strength (AU − cm^{-1}) observed	theory	% difference[g]
			1742	1742					
3270 ± 100	60	p	1723	1724			6.20	6.61	−6.2
	60	s	1718	1718	1744	1744	2.74	2.84	−3.5
	20	p	1719	1720	1747	1746	4.43	4.41	+0.5
	20	s	1719	1718	1746	1744	4.36	4.20	+3.8
362 ± 30	60	p	1742	1742			0.621	0.730	−14.9
	60	s	1715	1716	1736	1740	0.150	0.149	−0.7
	20	p	1718	1716	1738	1740	0.240	0.224	−7.1
	20	s	1715	1716	1742	1740	0.253	0.249	−1.6
78 ± 15	60	p	1740	1742				0.114	
	60	s	*e*	1715	*e*	1739	*e*	0.0243	
	20	p	*e*	1716	*e*	1738	*e*	0.0442	
	20	s	*e*	1716	*e*	1739	*e*	0.0466	

[a] Theoretical spectra calculated with classical electromagnetic theory (see text). [b] Uncertainties for thickness data given as the range of ellipsometric and/or surface profiler measurements. [c] Peak positions given to nearest integer value. [d] Two maxima observed in the spectrum for 3270 ± 100 Å PMMA/GC at $\theta_1 = 60°$ with p polarization. [e] These values could not be accurately estimated due to the low signal-to-noise ratio. [f] Integrated absorption strengths were calculated as $I = \int -\log (R/R_0)\, d\bar{\nu}$. [g] These values calculated as $[(I_{OBSERVED} - I_{THEORY})/I_{THEORY}] \times 100$.

PMMA/GC and R_0 is the reflectivity of bare GC; this ratio is the reflection analog of optical absorbance. In all instances, the observed band shapes are markedly distorted in comparison to those expected for transmission measurements. Absorbance maxima are about 10 cm^{-1} higher in energy than the transmission maximum, which is at 1731 cm^{-1}. In fact, the shoulder for the 380-Å and 78-Å films appears as a second absorbance maximum at 1723 cm^{-1} for the 3280-Å film. As discussed earlier, the band shape distortion results, in part, from the contribution of the anomalous dispersion of the PMMA refractive index and can be understood by considerations of the reflectivities for p- and s-polarized light.

Observed and calculated IR-ER spectra for the same three films are shown in Figure 5 for $\theta_1 = 60°$ with s polarization. These spectral band shapes differ dramatically from those for p-polarized light in Figure 4. The derivative-like shapes result from the predominant contribution of the dispersion of n_2. As such, the shapes strongly resemble the mirror image of n_2.

Observed and calculated IR-ER spectra obtained at $\theta_1 = 20°$ with p polarization and s polarization are shown for these films in Figures 6 and 7, respectively. As in Figure 5, the shapes and intensities are derivative-like and resemble the mirror image of n_2. The similarity of the band shapes and intensities for Figures 6 and 7 results from the near-equivalence of the MSEF for s and p polarization at $\theta_1 = 20°$ (see Figure 3).

Quantitative Aspects of IR-ERS. PMMA/GC. The comparison of observed and calculated PMMA/GC spectra provides a criterium for assessing the quantitative aspects of IR-ERS. As shown in Figures 4–7, the band shapes and intensities for the calculated spectra are very predictive of those observed. Table I details this comparison in terms of peak positions (maxima and/or minima) and integrated absorption strengths for the carbonyl vibration of PMMA. Observed and calculated positions agree in all instances to within 1–2 cm^{-1}. For example, both the observed and calculated spectra in Figure 4 for the 3270 ± 100 Å PMMA/GC at $\theta_1 = 60°$ with p polarization exhibit two maxima; the agreement between observed and calculated positions is within 1 cm^{-1}. Comparisons of the integrated absorption strengths show differences in all but one instance (362 ± 30 Å PMMA/GC at $\theta_1 = 60°$ with p polarization) that are less than about 7%. A plot of integrated absorption strength vs. PMMA thickness is nonlinear (for such large thicknesses) due to the periodicity of the MSEF. The results shown in Table I demonstrate the quantitative capabilities of IR-ERS and also indicate that comparisons between experimental and calculated spectra are requisite before assigning differences between IR-ER and transmission spectra to structure and/or chemical bonding changes of the film or interfacial structure.

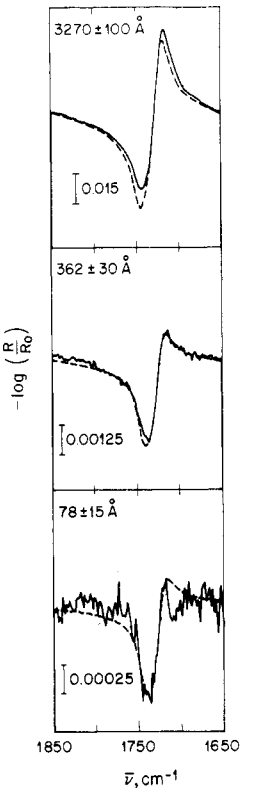

Figure 5. Experimental (——) and calculated (– – –) IR-ER spectra for PMMA films of various thicknesses at GC: 3270 ± 100 Å; 362 ± 30 Å; and 78 ± 15 Å. The s-polarized light is incident at 60°.

CONCLUSIONS

The quantitative aspects of IR-ERS for the characterization of thin polymer films at GC have been developed. Values of the MSEF as a function of angle of incidence, polarization, and substrate optical properties were used to determine

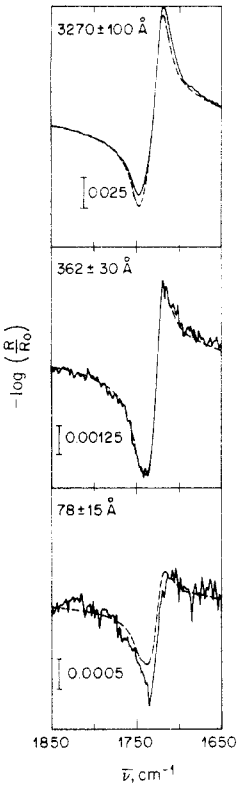

Figure 6. Experimental (——) and calculated (- - -) IR-ER spectra for PMMA films of various thicknesses at GC: 3270 ± 100 Å; 362 ± 30 Å; and 78 ± 15 Å. The p-polarized light is incident at 20°.

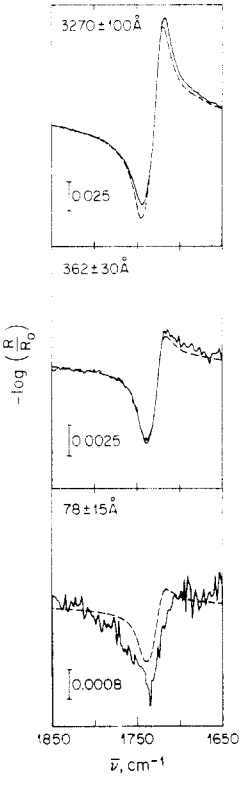

Figure 7. Experimental (——) and calculated (- - -) IR-ER spectra for PMMA films of various thicknesses at GC: 3270 ± 100 Å; 362 ± 30 Å; 78 ± 15 Å. The s-polarized light is incident at 20°.

conditions for optimum sensitivity and to examine the effects of the low reflectivity of GC on the band shapes and intensities. Comparisons of observed spectra and those calculated via classical electromagnetic theory provided the criteria for assessing the quantitative capabilities of IR-ERS. Such comparisons for several film thicknesses and experimental conditions of the C=O stretch for PMMA at GC generally give an agreement better than 93%. These results also indicate that considerations of the inherent differences between ERS transmission measurements are necessary before relating any band shape and intensity differences to structure and/or chemical bonding changes of the interfacial structure. Studies are in progress to extend these criteria to the quantitative analysis of structures at electrochemical interfaces, semiconductors, and insulators.

ACKNOWLEDGMENT

Helpful discussions with William M. Theis and George B. Norris are acknowledged.

Registry No. PMMA, 9011-14-7; C, 7440-44-0.

LITERATURE CITED

(1) Karweik, D. H.; Miller, C. W.; Porter, M. D.; Kuwana, T. In *Industrial Applications of Surface Analysis*; Casper, L. A., Powell, C. J., Eds.; American Chemical Society: Washington, DC, 1982; ACS Symp. Ser. No. 199.
(2) Murray, R. W. In *Electroanalytical Chemistry*; Bard, A. J., Ed.; Marcel Dekker: New York, 1984; Vol. 13.
(3) Lane, R. F.; Hubbard, A. T. *J. Phys. Chem.* **1973**, *77*, 1401–1410.
(4) Zak, J.; Kuwana, T. *J. Electroanal. Chem.* **1983**, *150*, 645–664.
(5) Landrum, H. L.; Salmon, R. T.; Hawkridge, F. M. *J. Am. Chem. Soc.* **1977**, *99*, 3154–3158.
(6) Willman, K. W.; Murray, R. W. *J. Electroanal. Chem.* **1982**, *133*, 211–231.
(7) Buttry, D. A.; Anson, F. C. *J. Am. Chem. Soc.* **1982**, *104*, 4824–4829.
(8) Ghosh, P. K.; Mau, A.; Bard, A. J. *J. Electroanal. Chem.* **1984**, *169*, 315–317.
(9) Wang, J.; Hutchins, L. *Anal. Chem.* **1985**, *57*, 1536–1541.
(10) Porter, M. D.; Karweik, D. H.; Kuwana, T.; Theis, W. M.; Norris, G. B.; Tiernan, T. O. *Appl. Spectrosc.* **1984**, *38*, 11–16.
(11) Datta, M.; Freeman, J. J.; Jansson, R. E. W. *Spectrosc. Lett.* **1985**, *1*, 273–282.
(12) Greenler, R. G.; Rahn, R. R.; Schwartz, J. P. *J. Catal.* **1971**, *23*, 42–48.
(13) Allara, D. L., Baca, A., Pryde, C. A. *Macromolecules* **1978**, *11*, 1215–1220.
(14) Greenler, R. G. *J. Chem. Phys.* **1966**, *44*, 310–315.
(15) Greenler, R. G. *J. Vac. Sci. Technol.* **1975**, *12*, 1410–1417.
(16) Harrick, N. J. *Internal Reflection Spectroscopy*; Wiley-Interscience: New York, 1967.
(17) Hansen, W. N. *J. Opt. Soc. Am.* **1968**, *58*, 380–386.
(18) Hansen, W. N. In *Advances in Electrochemistry and Electrochemical Engineering*; Delahay, P., Tobias, C. W., Eds.; Wiley: New York, 1973; Vol. 9.
(19) MacIntyre, J. D. E. In *Advances in Electrochemistry and Electrochemical Engineering*; Delahay, P., Tobias, C. W., Eds.; Wiley: New York, 1973; Vol. 9.
(20) Allara, D. L. In *Industrial Applications of Surface Analysis*; Casper, L. A., Powell, C. J., Eds.; American Chemical Society: Washington, DC, 1982; ACS Symp. Ser. No. 199.
(21) Golden, W. G. In *Fourier Transform Infrared Spectroscopy*; Academic Press: New York, 1985; Vol. 4.
(22) Schlotter, N. E.; Rabolt, J. F. *J. Phys. Chem.* **1984**, *88*, 2062–2067.
(23) Tompkins, H. G.; Allara, D. L. *Rev. Sci. Instrum.* **1974**, *45*, 1221–1222.
(24) Allara, D. L.; Nuzzo, R. G. *Langmuir* **1985**, *1*, 52–66.
(25) Graf, R. T.; Koenig, J. L.; Ishida, H. *Appl. Spectrosc.* **1985**, *39*, 405–408.
(26) Williams, M. W.; Arakawa, E. T. *J. Appl. Phys.* **1972**, *43*, 3460–3463.
(27) *CRC Handbook of Chemistry and Physics*; Weast, R. C.; Ed.; CRC Press: Cleveland, OH, 1973.
(28) Allara, D. L.; Swalen, J. D. *J. Phys. Chem.* **1982**, *86*, 2700–2704.
(29) Golden, W. G.; Snyder, C. D.; Smith, B. *J. Phys. Chem.* **1982**, *86*, 4675–4678.
(30) Rabolt, J. F.; Burns, F. C.; Schlotter, N. E.; Swalen, J. D. *J. Chem. Phys.* **1983**, *78*, 946–952.
(31) Baker, D. F.; Bragg, R. H. *J. Non-Crystalline Solids* **1983**, *58*, 57–69.

RECEIVED for review March 14, 1986. Accepted May 12, 1986. Portions of this work were performed at The Ohio State University with the support of the NSF-sponsored Materials Research Laboratory (M.D.P. and T.K.).